

Dwarf Dark Matter Halos

P. Colín

Instituto de Astronomía, Universidad Nacional Autónoma de México, C.P. 04510, México, D.F., México

A. Klypin, O. Valenzuela

Astronomy Department, New Mexico State University, Box 30001, Department 4500, Las Cruces, NM 88003-0001, U.S.A.

Stefan Gottlöber

Astrophysikalisches Institut Potsdam, An der Sternwarte 16, 14482 Potsdam, Germany

ABSTRACT

We study properties of dark matter halos at high redshifts $z = 2 - 10$ for a vast range of masses with the emphasis on dwarf halos with masses $10^7 - 10^9 h^{-1} M_\odot$. We find that the density profiles of *relaxed* dwarf halos are well fitted by the NFW profile and *do not have cores*. We compute the halo mass function and the halo spin parameter distribution and find that the former is very well reproduced by the Sheth & Tormen model while the latter is well fitted by a lognormal distribution with $\lambda_0 = 0.042$ and $\sigma_\lambda = 0.63$. We estimate the distribution of concentrations for halos in mass range that covers six orders of magnitude from $10^7 h^{-1} M_\odot$ to $10^{13} h^{-1} M_\odot$, and find that the data are well reproduced by the model of Bullock et al. The extrapolation of our results to $z = 0$ predicts that present-day isolated dwarf halos should have a very large median concentration of ~ 35 . We measure the subhalo circular velocity functions for halos with masses that range from $4.6 \times 10^9 h^{-1} M_\odot$ to $10^{13} h^{-1} M_\odot$ and find that they are similar when normalized to the circular velocity of the parent halo. Dwarf halos studied in this paper are many orders of magnitude smaller than well-studied cluster- and Milky Way-sized halos. Yet, in all respects the dwarfs are just down-scaled versions of the large halos. They are cuspy and, as expected, more concentrated. They have the same spin parameter distribution and follow the same mass function that was measured for large halos.

Subject headings: cosmology: theory — cosmology: dark matter — galaxies: formation — galaxies: halos — methods: numerical

1. Introduction

Dwarf galaxies with virial masses $10^7 - 10^9 M_\odot$ are the smallest virialized objects in the universe that show evidence of dark matter (Mateo 1998, and references therein). Some of these galaxies are so small that they can be detected only in the Local Group. Large amounts of dark matter along with the proximity to the Milky Way make dwarf galaxies an ideal laboratory for testing the hierarchical cosmologies such as the standard Λ CDM. The rotation curves of dwarf irregular galaxies

and the velocity dispersions of dwarf spheroidal galaxies have been used in the last decade to constrain the density of the dark matter in the central parts of these galaxies and, thus, to constrain the structure of dark matter (DM) halos that host the galaxies. So far the results indicate that DM halos should have flat cores (Carignan & Freeman 1988; Carignan & Beaulieu 1989; Flores & Primack 1994; Moore 1994; Burkert 1995). This is inconsistent with the cold dark matter theory, which predicts cuspy cores with $\rho \propto r^{-1}$ (Dubin-

ski & Carlberg 1991; Navarro, Frenk, & White 1995, 1996, 1997, hereafter NFW) or $\rho \propto r^{-1.5}$ (Moore et al. 1999). The controversy of the flat versus cuspy DM cores is still not resolved. Recent observations and analysis of dwarf and low surface brightness (LSB) galaxies rotation curves continue to suggest a dark matter halo density profile with a relatively flat core (de Blok, Bosma, & McGaugh 2003; Weldrake, de Blok, & Walter 2003), but see also Swaters et al. (2003); Rhee, Klypin, & Valenzuela (2003).

A second somewhat related problem faced by the CDM cosmogony is the excessive substructure predicted by this model in Milky Way-sized halos as compared with what is observed (Klypin et al. 1999b; Moore et al. 1999). Within the CDM framework this problem finds a natural explanation in the reionization of the universe: satellites form only inside subhalos that collapse early, before the universe was fully ionized (Bullock, Kravtsov, & Weinberg 2000; Somerville 2002; Benson et al. 2002). There may be a different reading of the substructure problem which depends on how peak circular velocities, v_{\max} , are assigned to dwarf spheroidal (dSph) galaxies (these galaxies comprise most of the Milky Way satellites). If these galaxies have a larger v_{\max} than what was previously expected, there is no disagreement: the small number of satellites would be explained by the relatively scarcity by which large subhalos are formed in the CDM model. In this case every large DM satellite hosts a dwarf galaxy. The absence of a stellar component in the numerous small DM satellites could be explained by feedback and/or reionization. The problem seems to be degenerate: observed dwarf galaxies can be hosted by either a relatively low-concentration but high- v_{\max} halo (Hayashi et al. 2003; Stoehr et al. 2002) or by a high-concentration and low- v_{\max} halo (Lokas 2002). Thus, the concentration of dwarf DM halos is quite important. Accurate measurements of the concentration for a large sample of dwarf DM halos is one of the goals of this paper.

Attempts have been made to simulate dwarf halos with high resolution within a cosmological context. Moore et al. (2001) simulated one “Draco”-sized halo ($M_{\text{vir}} \sim 10^8 h^{-1} M_{\odot}$) with several million particles and with high force resolution. Their fit of the density profile favor the inner slope -1.3 .

Ricotti (2002) presented several simulations including one with a small ($1 h^{-1} \text{Mpc}$) box. The dwarf halos in this small box are resolved with only few tens of thousands of particles at high redshifts. Ricotti (2002) finds that at $z \sim 10$ the density profiles have inner slopes in the range $[-0.4, -0.5]$. Recently, Cen et al. (2004) reproduced results of Ricotti (2002) using halos with very small number (few thousands) of particles. Cusps in these simulations are much flatter than that quoted by Moore et al. Navarro et al. (2003) made high resolution simulations of dwarf halos, but those were presented only at $z = 0$. Dwarf halos were found to have steep profiles. Thus, the issue of the evolution of the cusps of dwarfs is still not settled. Numerical effects are of special concern for low resolution simulations. Yet, there are other issues, which require attention including treatment of non-equilibrium features in the density distribution.

In this paper, we also study cusps of dwarf halos. But cusps is only one of the aspects, which we are interested in. The statistical properties of this population of halos such as the mass function or the spin parameter distribution are also studied.

Dwarf halos with masses $M_{\text{vir}} \sim 10^7 - 10^9 h^{-1} M_{\odot}$ studied in this paper form at very high redshifts. If a halo of this low mass remains isolated, it is expected to grow only 2-3 times since redshift $z \approx 3$ until $z = 0$ (van den Bosch 2002) with most of the mass ending up in the outer part of the halo. Thus, the halo profile should not change much since $z = 3$. The dwarfs may be accreted by larger halos and become satellites. If that happens, they are significantly stripped and lose most of their mass in outer regions. In any case, it is important to know what was the structure of the dwarfs at high redshifts. This is why we focus on the structure of the dwarfs at $z \approx 3$.

The paper is organized as follows. In §2 we present the cosmological model and describe numerical simulations used in our analysis. The mass function of simulated halos span a mass range of seven orders of magnitude. Density profiles of the most resolved dwarf halos from the $1 h^{-1} \text{Mpc}$ box are presented in §3.1. The concentration versus mass diagram along with the analytical prediction by Bullock et al. (2001a) is also shown there. In §3.2 we compute the subhalo velocity function for our most massive halos and show the almost self-

TABLE 1
PARAMETERS OF SIMULATIONS

| Box ($h^{-1}\text{Mpc}$) | Mass resolution ($h^{-1}\text{M}_\odot$) | Force resolution (comoving $h^{-1}\text{pc}$) | σ_8 | Name |
|-------------------------------|---|---|------------|------|
| 1 | 4.9×10^3 | 61 | 0.75 | A |
| 25 | 1.2×10^6 | 191 | 0.90 | B |
| 80 | 4.0×10^7 | 610 | 0.90 | C |
| 60 | 1.1×10^9 | 2000 | 1.00 | D |

similar nature of the dark matter inside virialized systems, in agreement with the results of Moore et al. (2001) and De Lucia et al. (2003). The differential mass function of halos from the $1 h^{-1}\text{Mpc}$ box is calculated in §4.1. A comparison is made with the prediction by Sheth & Tormen (1999). In §4.2 we calculate the spin parameter distribution of dwarf halos for the $1 h^{-1}\text{Mpc}$ box and compare it with one at $z = 0$ with the same cosmology. We discuss some of the results presented in previous sections and present our concluding remarks in §5.

2. Numerical Simulations

We use a series of simulations of a low-density flat ΛCDM cosmological model with the following parameters: $\Omega_0 = 0.3$, $\Omega_\Lambda = 0.7$, and $h = 0.7$. All simulations are done with the Adaptive Refinement Tree (ART) code (Kravtsov et al. 1997). The ART code achieves high spatial resolution by refining the base uniform grid in all high-density regions with an automated refinement algorithm.

For our code a convergence study shows that density deviations less than 10% are expected at radii larger than 4 times the formal force resolution or the radius that contains 200 particles, whichever is larger (Klypin et al. 2001). This is recently confirmed in a detailed analysis of halo profiles by Tasitsiomi et al. (2003). With the aim of studying the structure of dwarf halos, we perform a simulation of an $1 h^{-1}\text{Mpc}$ box on a side with 256^3 particles. One of the motivations for choosing this small box is to reproduce the same configuration as in Ricotti (2002). The simulation has been stopped at $z = 2.3$ when the longest fluctuations in the box are still well in the linear regime. At redshift $z = 3.3$ in the simulation there are 4 large halos resolved with more

than 200,000 particles and with proper force resolution $14h^{-1}\text{pc}$. For analysis we also use many more smaller halos.

To complement our study we use three more simulations. We use the simulation presented in Klypin et al. (2001), who focused on a convergence study of the density structure of three Milky Way-sized halos at low redshifts. At $z = 3$ the three largest halos in that simulation have a mass of about $10^{11} h^{-1}\text{M}_\odot$ and are resolved with $\sim 10^5$ particles. For our analysis we also use 12 large halos with more than 5000 particles ($M > 6 \times 10^9 h^{-1}\text{M}_\odot$).

We also use a 80 $h^{-1}\text{Mpc}$ box simulation, in which at redshift $z = 3$ we identified 5 large halos resolved with more than 10^5 particles. At $z = 0$ the halos have become a cluster-sized halo of virial mass $M_{vir} \approx 2 \times 10^{14} h^{-1}\text{M}_\odot$. The high redshift halos are used for our analysis.

Finally, we use the 60 $h^{-1}\text{Mpc}$ simulation with 256^3 particles described in Colín et al. (1999); Klypin et al. (1999a). The parameters of all the simulations are presented in Table 1. In column 1 we show the comoving size of the computational box. The mass resolution is given in column 2, while the formal spatial resolution (size of a cell in the finest refinement grid in comoving units) is shown in column 3. Column 4 gives the value of σ_8 (the rms of mass fluctuations estimated with the top-hat window of radius $8h^{-1}\text{Mpc}$). Finally, column 5 gives the name of the simulation (which is also used for objects studied in this simulation).

In our simulations the halos are identified by the Bounded-Density-Maxima (BDM) algorithm (Klypin & Holtzman 1997; Klypin et al. 1999a). The BDM algorithm first finds positions of local maxima in the density field. These density

maxima are found using a top-hat filter with a “search radius” which is several times larger than the force resolution. Once centers of potential halos are found, the algorithm identifies halos around them and removes particles which are not bound to those halos. This procedure also detects subhalos of larger objects – halos inside halos (for example, satellites of galaxies or galaxies in clusters). Particles of a subhalo are bound to both the subhalo and to the larger halo.

3. Halo structure

3.1. Density profiles and concentrations

We start our analysis of halo profiles by studying all most massive halos (subhalos are not included). The profiles are not averaged over time and halos are not selected to be quite or not to have large merging events. Thus, some non-equilibrium features are expected. Figure 1 shows the density profiles of the ten most massive halos in the $1h^{-1}\text{Mpc}$ box at $z = 3.3$ plotted from the radii which contain at least 200 particles to their virial radii. The profiles are given in normalized units: the radius is measured in units of the scale radius r_s , the radius where the logarithmic derivative of the NFW profile (see equation 1) is equal to -2 , whereas the density is measured in units of a characteristic density $\rho_s = \rho_0/4$, the NFW density evaluated at $r = r_s$. These parameters are taken from their corresponding NFW fits. The halos show a variety of profiles. Some profiles have significant deviations from the NFW fit (e.g., the second and the forth from the top) while others are fitted by NFW reasonably well (e.g., the fifth halo).

The wiggles in the profiles seen in the outskirts of most halos can be explained as substructure that have not yet reached equilibrium with the rest of the halo or as the result of a significant merger. For example, halos number 2 and 9 from top are in the process of a major merger. Both halos show a density enhancement in the peripheral part (more pronounced in case of halo 2). The almost power-law profile of halo 9 may be a consequence of the way the merger has developed ¹.

¹Out of the fifteen biggest halos in the $1 h^{-1}\text{Mpc}$ box, the merger companion of halo 9 has the most peculiar density profile. It has the highest r_s value even though it is the

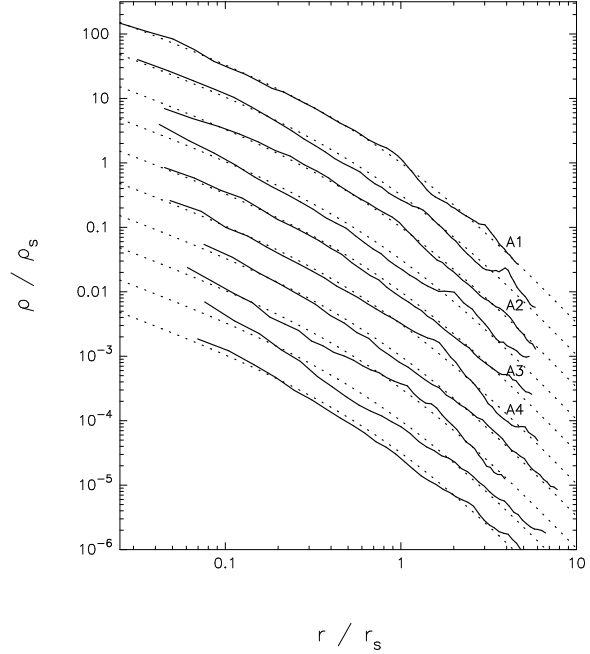


Fig. 1.— Density profiles of the ten most massive halos of the $1 h^{-1}\text{Mpc}$ box in normalized units. The dotted curves are the NFW profile. For clarity we shift down the profiles by -0.5 in logarithm. Halos are ordered by mass with the most massive halo being at the top of the plot. The density profiles are cut at the virial radii. The innermost bin contains more than 200 particles. No sign of a shallow core is seen in any of the halos. However, most halos have wiggles in the peripheral regions, which are due to residual substructure and ongoing merging. The labels A_n , with $n = 1, \dots, 4$, represent the “equilibrium” halos used for subsequent analysis.

No matter how large or small are the deviations, the profiles do not show a sign of flat cores in the central part of dwarf halos. In other words, steep central cusps of halos in our simulations contradict the results of Ricotti (2002), who finds that central slopes of halos in his $1 h^{-1}\text{Mpc}$ simulation are very shallow: $\rho \propto r^\alpha$, $\alpha \approx -0.2$.

There are some differences in the way how we and Ricotti (2002) approximate profiles. Ricotti does the approximations at much earlier time $z \sim 10$ when halos are much smaller and are less

second least massive halo on the list.

TABLE 2
PARAMETERS OF THE MOST MASSIVE HALOS AT $z \approx 3$

| M_{vir} ($h^{-1}M_{\odot}$) | r_{vir} ($h^{-1}\text{kpc}$) | N_{part} | v_{max} (km/s) | r_s (proper $h^{-1}\text{kpc}$) | ρ_0 (proper $M_{\odot}h^2 \text{ pc}^{-3}$) | Halo name |
|------------------------------------|-------------------------------------|------------|----------------------------|---------------------------------------|--|-----------|
| 4.6×10^9 | 9.3 | 933636 | 48 | 2.0 | 5.0×10^{-2} | A1 |
| 1.4×10^9 | 6.6 | 285651 | 34 | 1.1 | 7.8×10^{-2} | A2 |
| 1.1×10^9 | 6.1 | 227275 | 28 | 1.1 | 6.6×10^{-2} | A3 |
| 1.0×10^9 | 6.0 | 208005 | 31 | 1.0 | 7.6×10^{-2} | A4 |
| 2.9×10^{11} | 41.7 | 238083 | 190 | 7.1 | 5.8×10^{-2} | B1 |
| 1.2×10^{11} | 30.8 | 95899 | 128 | 12.2 | 9.2×10^{-3} | B2 |
| 1.1×10^{11} | 29.9 | 86832 | 136 | 4.4 | 8.2×10^{-2} | B3 |
| 1.2×10^{13} | 140.0 | 288061 | 647 | 26.9 | 4.8×10^{-2} | C1 |
| 6.9×10^{12} | 117.3 | 175882 | 497 | 57.2 | 6.0×10^{-3} | C2 |

resolved. Instead of making two-parameter fits as we do, Ricotti uses a very simple approach: he uses “location and value of the maximum circular velocity”. When we apply the same prescription to our high resolution profiles at $z = 3$, we get very noisy results with fits going either above or below actual profiles. Yet, we did not get systematic effects. In Figure 2 we show the density profiles of the 6 most massive halos at $z = 10.5$ fitted with NFW profiles using two free parameters. The NFW fits approximate reasonable well the density profiles. Even without any fits it is clear that none of the profiles are even close to the shallow profiles suggested by Ricotti.

In the subsequent analysis we mostly focus on equilibrium halos, which are fitted by the NFW profile. Table 2 presents parameters of the most massive halos identified in the simulations A – C at redshift $z \sim 3$. In column 1 we show the mass M_{vir} within the virial radius (column 2). Here and below we present radii and densities in proper units. The virial radius, r_{vir} , is defined as the radius where the average halo density is δ times the background density according to the spherical top-hat model. Here δ is a number that depends on epoch and cosmological parameters ($\Omega_0, \Omega_{\Lambda}$); for a flat Λ CDM model, $\delta \sim 180$ at $z = 3$. In column 3 the corresponding number of particles is given. The maximum circular velocity $v_{\text{max}} = (GM(< r)/r)^{1/2}$, where G is the gravitational constant and $M(< r)$ is the mass within the radius r , is located in column 4. In column 5 and 6 we

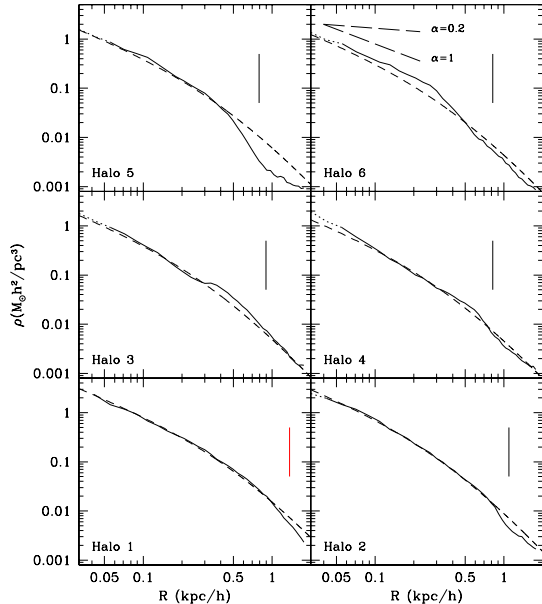


Fig. 2.— Density profiles of the most massive halos at $z = 10.5$ (full curves). Dashed curves show NFW fits. Long-dashed lines in the plot of Halo 6 show power-laws with slopes $\alpha = 1$ (NFW) and $\alpha = 0.2$ (Ricotti). In spite of large fluctuations at large (virial) radii, none of the halos show slopes suggested by Ricotti (2002).

present the NFW parameters r_s and ρ_0 in proper units. The name of the halos are given in the last column.

We impose the following “equilibrium” criteria to select a halo for further analysis: (1) The halo should not be within the virial radius of a more massive halo; i.e, the halo is not a subhalo. (2) The halo should not have a subhalo with a mass larger than one tenth the mass of the halo. Finally, (3) we also use a goodness of fit criterion to reject halos with $D_f \geq 0.004$, where the accuracy of the fit D_f is defined as follows.

We compute the density, $\rho(r)$, in spherical shells whose radii increase as the square of the bin number, n . Under this scheme, the logarithmic radial width, $\Delta \log r$, is not constant but decreases with n , and for high values of n $\Delta \log r$ goes as $2/n$. This binning improves the often used constant logarithmic binning. We use the NFW profile, ρ_{NFW} , to fit our halo density profiles

$$\rho_{\text{NFW}}(r) = \frac{\rho_0}{r/r_s(1+r/r_s)^2}. \quad (1)$$

The best fit and thus parameters ρ_0 and r_s are obtained by minimizing χ^2 ,

$$\chi^2(\rho_0, r_s) = \sum_{n=1}^N \left[\frac{\log \rho(r_n) - \log \rho_{\text{NFW}}(r_n)}{\sigma_n} \right]^2. \quad (2)$$

We define $\omega_n \equiv 1/\sigma_n^2$ to be

$$\omega_n = \frac{\Delta r}{r_n} = \frac{2n+7}{(n+3)^2} \quad (3)$$

to compensate for the increasing density of bins with radius. In equation (3), Δr is the radial width for our binning scheme and n is the number of the bin corresponding to radius r_n . Notice that by definition ω is constant for a binning constant in $\log(r)$. We estimate the accuracy of the fit with the parameter $D \equiv \chi^2/F$, where $F = \sum \omega_n$ and the sum runs over the number of bins N . This parameter reduces to χ^2/N (with $\sigma_n = 1$) when ω is constant and it is a better estimation of the goodness of the fit than, for example, a maximum deviation because average out possible large fluctuations in some bins. We set $D = D_f = 0.004$ as our criterion for the quality of the fit. Halos with $D_f < 0.004$ that satisfy at the same time our minimum requirements for equilibrium (criteria 1 and 2) comprise 65% of the sample. In fact, in the distribution of D there is a strong drop in the number of halos above D_f . It seems that D_f separates relaxed from unrelaxed halos.

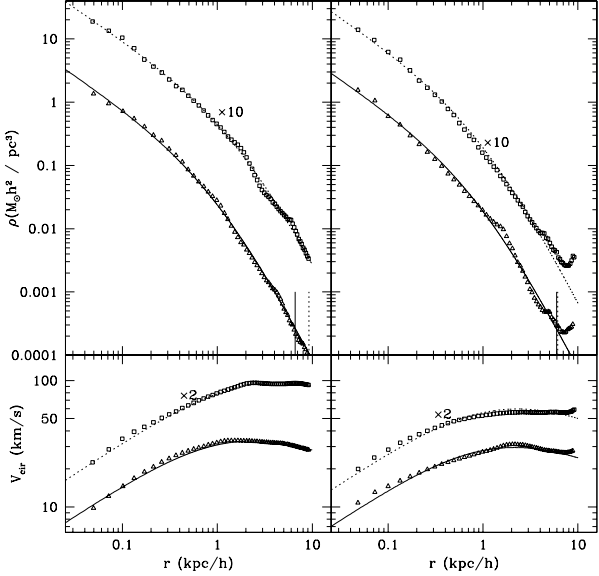


Fig. 3.— Density and circular velocity profiles of the four most massive halos at $z = 3.3$ that satisfy our criteria of “equilibrium” halos. The densities of the first (A1, left panel) and third (A3, right panel) halos have been multiplied by ten to prevent overlapping. The corresponding circular velocities (lower panel) were multiplied by a factor of two. The innermost bin is chosen to contain at least 200 particles. Vertical lines at the bottom of the density panels mark the corresponding virial radii (A1, A3 - dotted lines, A2, A4 solid lines)

Figure 3 shows the density and circular velocity, V_c , profiles for the four most massive halos of the $1 h^{-1}\text{Mpc}$ box that satisfy the criteria of “well-behaved” or “equilibrium” halos (A1 – A4). Dotted and solid lines are the NFW best fits. NFW circular velocity profiles are computed using (ρ_0, r_s) parameters obtained from the density fits. The NFW profile describes quite well both the density and the circular velocity profiles of these halos. At redshift $z \sim 3$ the majority – about 65% – of dwarf halos with more than 5000 particles are in “equilibrium”.

Figure 4 shows the inner structure of the most massive halo A1 (density, circular velocity and 3D velocity dispersion profiles) for epochs from $z = 11.5$ to $z = 2.3$. The virial mass of the halo increases 71 times during the period. Yet, the inner

density profile (radii less than ≈ 100 pc) changes very little. Thus, the cusp of the halo was already in place at very high redshift and since then shows little evolution. The central 0.5 kpc region shows little evolution since redshift $z = 5$. This does not mean that particles, which at redshift $z \approx 10$ are in the core stay there at later times. Comparison of the rms velocities (middle panel) with the circular velocities (top panel) clearly indicates that particles in the core move with random velocities that significantly exceed the circular velocity. This implies that the core itself is not self-bound and a large fraction of particles simply passes through the cusp. This is very important for understanding the evolution of halo concentration.

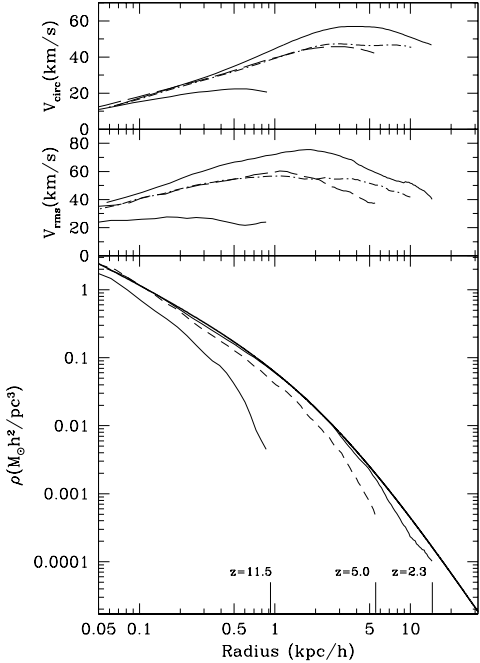


Fig. 4.— Circular velocity, 3D velocity dispersion, and density profiles of the most massive halo A1 at different redshifts. Dot dashed curves on the top two panels are for $z = 3.3$. For clarity we do not show the density profile for this redshift. Vertical lines in the bottom panel mark the virial radii. Most of the changes happen at outer radii of the halo while there is very little evolution in the center. The thick full curve in the bottom panel shows the NFW fit for $z = 2.3$.

For analysis of halo concentrations we make fits

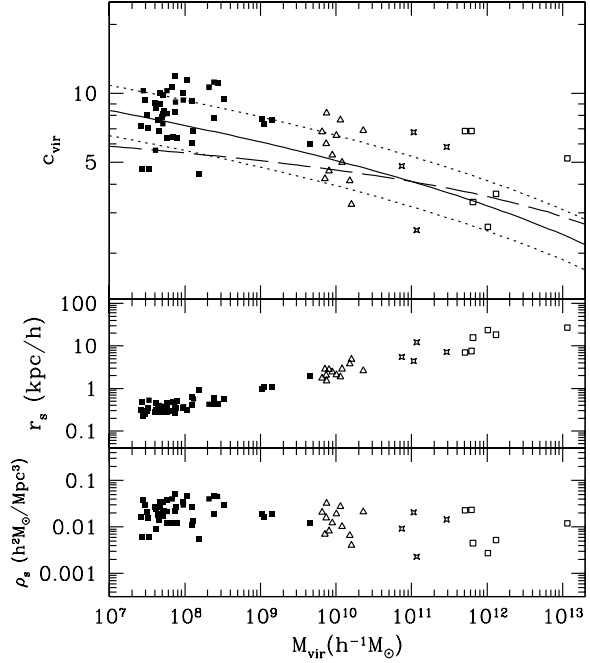


Fig. 5.— The dependence of concentration (c_{vir} , top panel), the scale radius (r_s , middle panel) and $\rho_s = \rho_0/4$ (ρ_s , bottom panel) on the halo virial mass. Solid squares are halos in the $1 h^{-1} \text{Mpc}$ box at $z = 3.3$. The rest of the points are for halos in the $25 h^{-1} \text{Mpc}$ simulation (open triangles and four-point stars) and the $80 h^{-1} \text{Mpc}$ simulation (open squares) at $z = 3$. The solid and dashed curves represent the predictions of the models by Bullock et al. (2001a) and Eke, Navarro, & Steinmetz (2001), respectively, while the dotted lines are the 1σ scatter of halos from the $1 h^{-1} \text{Mpc}$ box, $\Delta(\log c_{vir}) = 0.11$.

for halos with more than 5000 particles in all our simulations. At $z = 3.3$ in the $1 h^{-1} \text{Mpc}$ box simulation there are 72 of these halos of which 40 satisfy the equilibrium criteria. We also include seven more halos that do not satisfy the second criterion (have large companion), but are still well fitted by the NFW profile. Halos selected in the other two simulations also have more than 5000 particles each and the deviations of the measured density profile from the NFW fit are less than 30%; $|\rho(r_i) - \rho_{\text{NFW}}(r_i)| / \rho_{\text{NFW}}(r_i) < 0.3$, where r_i goes from the first radial bin to r_{vir} . Halos that are too disturbed hardly satisfy this latter “equilibrium” requirement (Jing 2000). Figure 5

shows concentrations $c_{vir} \equiv r_{vir}/r_s$, proper scale radii, r_s , and proper densities at the scale radii $\rho_s = \rho_0/4$ for halos of different virial masses M_{vir} . The solid and dashed curves are the predictions of the concentration at $z = 3.0$ based on the models of Bullock et al. (2001a) and Eke, Navarro, & Steinmetz (2001), respectively, for the appropriate cosmological model with $\sigma_8 = 0.9$. The points from the $1 h^{-1}\text{Mpc}$ box are slightly scaled up to take into account the different normalization ($\sigma_8 = 0.75$) and the slightly different identification redshift ($z = 3.3$). For this latter, we use the $1 + z$ dependence of c_{vir} while for the former we multiply c_{vir} by $0.9/0.75$, which is a good approximation because dwarf halos form very early when the growth factor is proportional to a .² We use the halos from the $1 h^{-1}\text{Mpc}$ box to compute the standard deviation of the $\log(c)$ distribution and find $\Delta(\log c_{vir}) = 0.11$, which is a factor 1.6 lower than that quoted by Bullock et al. (2001a). If we use the whole sample of halos only under the restriction that they must have more than 5000 particles, the scatter increases to 0.14. So, at least part if not all (see §5), of our smaller scatter is due to the fact that we are using relaxed halos.

In summary, dwarf halos seem to be in many respects a down-scaled copy of more massive halos. For example, they all have cusps regardless of their equilibrium status. Interestingly, they have a median concentration that agree with the model of Bullock et al. (2001a). We extended the c_{vir} versus M_{vir} diagram to high masses and showed how the Bullock et al. model continue to predict the correct concentration.

3.2. Substructure mass function

The cumulative velocity function of subhalos within halos A1 (open circles), B1 (open triangles), and C1 (solid circles) are compared in Figure 6. The peak velocities of subhalos are measured in units of the virial velocity, defined as the circular velocity at the virial radius, of their parent halo. The mass of the halos covered almost four orders of magnitude yet the subhalo velocity distributions are similar (Moore et al. 2001; De Lucia et al.

²Bullock et al. (2001a) define the epoch of collapse as the epoch at which the non-linear mass, M_* , equals a fixed fraction F of the halo mass, M_{vir} . For the ΛCDM model, Bullock et al. suggest to use $F = 0.01$.

2003). This function can be approximated by a power-law with power index -2.75 (Klypin et al. 1999b) (see dot-dashed line in Figure 6).

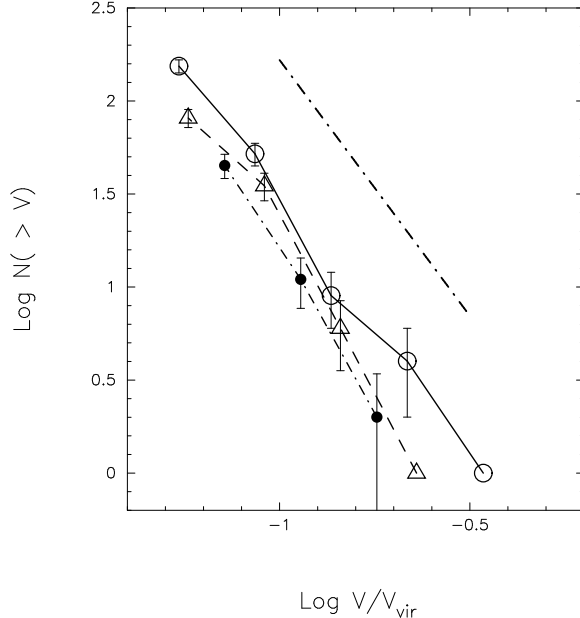


Fig. 6.— The cumulative number of subhalos with given circular velocity for halos A1 (open circles), B1 (open triangles), and C1 (solid circles). At $z \sim 3$ each halo has more than 2×10^5 particles and is resolved down to radius $0.01r_{vir}$ (the first radial bin with > 200 particles). The subhalo maximum circular velocities are in units of the virial velocity of the parent halo. The dot-dashed line shows the power law with the slope -2.75 found in previous simulations.

4. Statistics of halos

4.1. Halo mass function

The mass function of halos $N(M)$ is defined so that $N(M)dM dV$ represents the number of halos with masses between M and $M + dM$ in the volume dV . This is a differential mass function. In order to find isolated halos we use the friends-of-friends group finding algorithm (Davis et al. 1985) with a linking length of 0.2 (or in physical units $0.78 h^{-1}\text{kpc}$). Halos are identified as the set of particles mutually linked. The mass of the halo is simply the sum of its constituent dark matter particles. Tests (e.g., Governato et al. 1999)

indicate that at least 30 particles are needed to take into account properly the effect of mass resolution. In this paper we analyze only halos with more than 40 particles.

We construct the dwarf halo mass function by grouping the halos according to their mass in bins of $\Delta \log(M) = 0.1$. In order to avoid too large statistical fluctuations, we do not use the few most massive halos. Error bars for data in individual bins are estimated using Poisson statistics.

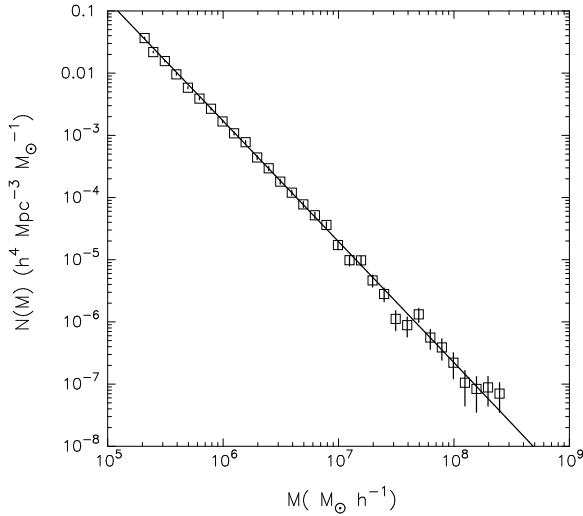


Fig. 7.— The halo mass function from the $1 h^{-1}\text{Mpc}$ box (open squares). Error bars are computed assuming the Poisson statistics. The solid line is the analytical prediction from the Sheth-Tormen formalism.

Figure 7 shows the mass function (open squares) of our dwarf halos from the $1 h^{-1}\text{Mpc}$ box. The solid line is the analytical prediction of the mass function from the Sheth-Tormen formalism. Notice the excellent agreement between the prediction of the Sheth-Tormen model and our numerical results. This model has been tested under diverse conditions: redshifts, cosmological parameters, halo masses ($> 10^{10} h^{-1}\text{M}_\odot$), etc., and have passed all tests (but see Reed et al. 2003). Here we see that it successfully predicts the mass function of dwarf halos, albeit at high redshift. In summary, the Sheth-Tormen formalism can be safely applied in different cosmological models and for about ten orders of magnitude in mass. With the corresponding correction factors the Sheth-Tormen formalism can be successfully applied also to pre-

dict the number of dwarfs in voids (Gottlöber et al. 2003).

4.2. Spin parameter distribution

To study the distribution of the spin parameter, $p(\lambda)$, we use halos which do not reside inside a larger halo and have more than 500 particles. The spin parameter λ is defined by

$$\lambda \equiv \frac{J |E|^{1/2}}{GM^{5/2}}, \quad (4)$$

where J is the magnitude of the angular momentum, E is the total energy, and M is the mass of the halo. We assume that halos are in virial equilibrium and thus $E = -K$, where K is the kinetic energy inside r_{vir} . N-body simulations have shown that $p(\lambda)$ is well described by a lognormal distribution (see Vitvitska et al. (2002) and references therein)

$$p(\lambda)d\lambda = \frac{1}{\sigma_\lambda \sqrt{2\pi}} \exp\left[-\frac{\ln^2(\lambda/\lambda_0)}{2\sigma_\lambda^2}\right] \frac{d\lambda}{\lambda}. \quad (5)$$

Figure 8 compares the probability distributions of the spin parameter in simulations A and D (Table 1) and shows the lognormal fits.

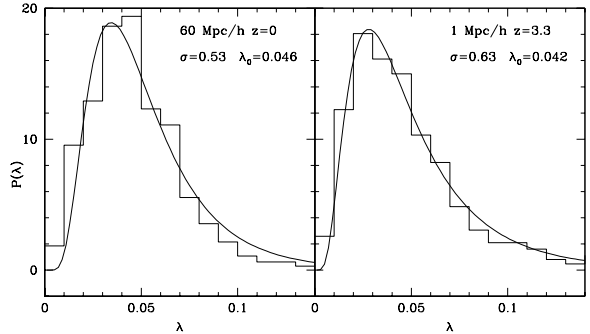


Fig. 8.— Spin parameter distribution (histogram) for halos with more than 500 particles drawn from a $60 h^{-1}\text{Mpc}$ box simulation at $z = 0$ (left panel) and from our $1 h^{-1}\text{Mpc}$ box at $z = 3.3$ (right panel). Curves on each panel are lognormal best-fits to the data. The parameters of the fit ($\sigma_\lambda, \lambda_0$) are also shown in panels.

Figure 8 shows that the distribution of the spin parameter of dwarf halos also follows a lognormal law. In fact, it turns out that dwarf halos in simulations A are better described by equation (5) than

the more massive halos in the simulation D: their distribution has a lower χ^2 for the same number of bins. According to the values of the parameters of the fit, it would appear that the distributions are different, but within the errors they are similar. What happens is that $p(\lambda)$ is very sensitive to $(\sigma_\lambda, \lambda_0)$. In general, our results confirm the known independence of the spin parameter on mass (Lemson & Kauffmann 1999) and epoch (e.g., Vitvitska et al. 2002).

5. Discussion and conclusions

We find that the density profiles of relaxed dwarf halos can be well fitted by the NFW profile, which has an inner density slope $\alpha = -1$. This result is in conflict with results of Ricotti (2002), who finds $\alpha \approx -0.5$ for dwarf halos in his $1 h^{-1}\text{Mpc}$ box simulation. In a attempt to find the cause of our discrepancy, we studied density profiles at the same redshift as Ricotti did ($z = 10.5$) and reproduced Ricotti's fitting procedure. The conclusion is that even without any fits none of the profiles are close to the shallow profiles suggested by Ricotti. On the other hand, Navarro et al. (2003), in a recent study of mass profiles of ΛCDM halos at $z = 0$ that span five decades in halo mass, show that inner density slopes of dwarf halos are steeper than -1 all the way down to the resolution limit. From their Tables 2 and 3 we find dwarf halo concentrations from $c_{vir} = 16.4$ for halo D1 to $c_{vir} = 22.0$ for halo D4. These concentrations are below to our extrapolated value of the median concentration we find for our dwarf halos, but once the mass dependence of the concentration is considered they turn out to be similar. Our results thus agree with the study of Navarro et al. on dwarf halos not only in the inner shape of density profiles but also on concentrations.

It is impressive to see how well the model of Bullock et al. (2001a) reproduces over five orders of magnitude the measured concentration as a function of halo mass. At the same time, Bullock et al. overpredict the deviations from the mean value. We compute the median and standard deviation of the c_{vir} distribution of our sample of relaxed dwarf halos and find a spread which disagrees with that reported in Bullock et al. by about a factor 1.6 in $\Delta \log c_{vir}$. It appears that the printed version of Bullock et al. has a typo and the

actual value for the spread of concentration in Bullock et al. should have been $\Delta \log c_{vir} = 0.14$ (Bullock, private communication). This is still larger than what we found: $\Delta \log c_{vir} = 0.11$. Our 1σ scatter is close to $\Delta \log c_{vir} = 0.10$ measured by Klypin et al. (2003). We found that, except at the high-mass end, Eke's et al. model lie below Bullock's et al. For instance, at $M_{vir} = 10^7 h^{-1}\text{M}_\odot$ Bullock's et al. model predicts $c_{vir} = 8.8$ as compared with 5.5 of Eke's et al. model.

If we extrapolate the concentration of our dwarf halos to the present using the $1+z$ growth law of the Bullock et al. model, the median would be about 30. This is higher; for example, than the value $c_{200} \sim 14$ (or $c_{vir} \sim 18$, no mass loss case) used by Hayashi et al. (2003). A shift up in c_{200} in Hayashi et al. fitting procedure would reduce the lower limit in v_{\max} ; that is, a lower v_{\max} would be required to match the observed stellar velocity dispersion of Carina and Draco. In any case, it is not clear to what extent Hayashi et al. results can be applied to the observed satellites when substructure is constrained to evolve in a static potential. Stoehr et al. (2002), on the other hand, are able to explain the observed central velocity dispersions of the dSph satellites of the Milky Way-sized galaxy halo. Subhalos are resolved with hundreds or at most with a few thousands of particles. These still small numbers of particles are probably not enough to draw yet firm conclusions. In the light of our results, it seems that subhalos resolved with many more particles than subhalos in present-day cosmological simulations will be more concentrated. However, it is not clear how this effect will affect the conclusion that observed dSph galaxies inhabit the largest subhalos.

In our analysis of the structure of dwarf halos, we also compute the abundance of subhalos. We measure the amount of substructure in halos A1 (dwarf halo), B1 (Magellanic Cloud-sized halo) and C1 (group-size halo) through the normalized subhalo v_{\max} function (v_{\max} is measured in units of the virial velocity of the parent halo) and find a mass-scale independent result: the curves are similar and well approximated by the power-law $n(> V) \propto V^{-2.75}$ (Klypin et al. 1999b). This is in agreement with the paper by Moore et al. (2001) (see also De Lucia et al. (2003)).

We compute the dwarf halo mass function and

find an excellent agreement with the model of Sheth & Tormen (1999). The model has been tested at different redshifts, for a variety of cosmologies, and for halo masses above $\sim 10^{10} h^{-1} M_{\odot}$ (Sheth & Tormen 1999; Jenkins et al. 2001; Reed et al. 2003). It provides an excellent match to the data. In this paper, we tested it at much lower masses, $10^5 - 10^8 h^{-1} M_{\odot}$, and found also an excellent agreement with the data. It is pleasant to know that this approximation is able to match data for ten orders of magnitude in mass.

The spin parameter distribution $p(\lambda)$ is measured for our sample of dwarf halos (halos with a virial mass between 10^7 and $10^9 h^{-1} M_{\odot}$). It is well fitted by a lognormal distribution with $\lambda_0 = 0.042$ and $\sigma_{\lambda} = 0.63$. These parameters roughly agree with those estimated by Vitvitska et al. (2002). Our results corroborate the known independence of the spin parameter on mass (Lemson & Kauffmann 1999) and epoch (e.g., Vitvitska et al. 2002).

Acknowledgement: P.C. acknowledge support by CONACyT grant 36584-E, S.G. and A.K. by NSF/DAAD, S.G. and P.C. by DFG/CONACyT. Computer simulations presented in this paper were done at the Leibnizrechenzentrum (LRZ) in Munich and at the National Energy Research Scientific Computing Center (NERSC). We thank J. Bullock and V. Avila-Reese for helpful comments and discussions. We acknowledge the anonymous referee whose helpful comments and suggestions improved some aspects of this paper.

REFERENCES

Benson, A.J., Frenk, C.S., Lacey, C.G., Baugh, C.M., & Cole, S. 2002, MNRAS, 333, 177

Bond, J.R., Cole, Efstathiou, G., & Kaiser, N. 1991, apJ, 379, 440

Bullock, J.S., Kravtsov, A.V., & Weinberg, D.H. 2000, ApJ, 539, 517

Bullock, J.S., Kolatt, T.S., Sigad, Y., Somerville, R.S., Kravtsov A.V., Klypin, A.A., Primack, J.R., & Dekel, A. 2001a, MNRAS, 321, 559

Bullock, J.S., Dekel, A., Kolatt, T.S., Kravtsov, A.V., Klypin, A.A., Porciani, C., & Primack, J.R. 2001, ApJ, 555, 240

Burkert, A. 1995, ApJ, 447, L25

Carignan, C., & Beaulieu, S. 1989, ApJ, 347, 760

Carignan, C., & Freeman, K.C. 1988, ApJ, 332, L33

de Blok, W.J.G., Bosma, A., & McGaugh, S. 2003, MNRAS, 340, 657

Cen, R., Dong, F., Bode, P., & Ostriker, J.P. ApJ submitted (astro-ph/0403352)

Colín, P., Klypin, A.A., Kravtsov, A.V., & A.M. Khokhlov. 1999, ApJ, 523, 32

De Lucia, G., Kauffmann, G., Springel, V., & White, S.D.M. MNRAS submitted (astro-ph/0306205)

Davis, M., Efstathiou, G., Frenk, C.S., & White, S.D.M. 1985, ApJ, 292, 371

Dubinski, J., & Carlberg, R. 1991, ApJ, 378, 496

Eke, V.R., Cole, S., Frenk, C.S. 1996, MNRAS, 282, 263

Eke, V.R., Navarro, J.F., & Steinmetz, M. 2001, ApJ, 554, 114

Flores, R.A., & Primack, J.R. 1994, ApJ, 427, L1

Gottlöber, S., Lokas, E., Klypin, A.A., Hoffman Y. 2003, MNRAS, in press

Governato, F., Babul, A., Quinn, T., Tozzi, P., Baugh, C.M., Katz, N., & Lake, G. 1999, MNRAS, 307, 949

Hayashi, E., Navarro, J.F., Taylor, J.E., Stadel, J., & Quinn, T. 2003, ApJ, 584, 541

Jenkins, A., Frenk, C.S., White, S.D.M., Colberg, J.M., Cole, S., Evrard, A.E., Couchman, H.M.P., & Yoshida, N. 2001, MNRAS, 321, 372

Jing, Y.P. 2000, ApJ, 535, 30

Klypin, A.A., Holtzman, J., 1997, <http://xxx.lanl.gov/pdf/astro-ph/9712217>

Klypin, A.A., Gottlöber, S., Kravtsov, A.V., & Khokhlov, A.M 1999, ApJ, 516, 530

Klypin, A.A., Kravtsov, A.V., Valenzuela, O., & Prada, F. 1999, ApJ, 522, 82

Klypin, A.A., Kravtsov, A.V., Bullock, J.S., & Primack, J.R. 2001, ApJ, 554, 903

Klypin, A.A., Macció, A.V., Mainini, R., & Bonometto, S.A. 2003, ApJ submitted (astro-ph/0303304)

Kravtsov, A.V., Klypin, A.A., & Khokhlov, A.M., 1997, ApJS, 111, 73

Lemson, G., & Kauffmann, G. 1999, MNRAS, 302, 111

Lokas, E.L. 2002, MNRAS, 333, 697

Mateo, M. 1998, ARA&A, 36, 435

Moore, B. 1994, Nature, 370, 629

Moore, B., Quinn, T., Governato, F., Stadel, J., & Lake, G. 1999a, MNRAS, 310, 1147

Moore, B., Ghigna, S., Governato, F., Lake, G., Quinn, T., Stadel, J., Tozzi, P. 1999b, ApJ, 524, 19

Moore, B., Calcáneo-Roldán, C., Stadel, J., Quinn, T., Lake, G., Ghigna, S., & Governato, F. 2001, PhRvD, 64, 063508

Navarro, J.F., Frenk, C.S., & White, S.D.M. 1995, MNRAS, 275, 720

Navarro, J.F., Frenk, C.S., & White, S.D.M. 1996, ApJ, 462, 563

Navarro, J.F., Frenk, C.S., & White, S.D.M. 1997, ApJ, 490, 493

Navarro, J.F., Hayashi, E., Power, C., Jenkins, A.R., Frenk, C.S., White, S.D.M., Springel, V., Stadel, J., & Quinn, T.R. 2003, MNRAS submitted (astro-ph/0311231)

Ricotti, M. 2003, MNRAS, 344, 1237

Peebles, P.J.E. 1980, The Large Scale Structure of the Universe (Princeton: Princeton Univ. Press)

Reed, D., Gardner, J., Quinn, T., Stadel, J., Fardal, M., Lake, G., & Governato, F. 2003, MNRAS submitted (astro-ph/0301270)

Rhee, G., Klypin, A., & Valenzuela, O. 2003, in preparation

Sheth, R., & Tormen, G. 1999, MNRAS, 308, 119

Somerville, R. 2002, ApJ, 572, L23

Stoehr, F., White, S.D.M., Tormen, G., & Springel, V. 2002, MNRAS, 335, L84

Swaters, R.A., Madore, B.F., van den Bosch, F.C., & Balcells, M. 2003, ApJ, 583, 732

Tasitsiomi, A., Kravtsov, A.V., Gottlöber, S., & Klypin, A.A. 2003, ApJ submitted (astro-ph/0311062)

van den Bosch, F. C. 2002, MNRAS, 331, 98

Vitvitska, M., Klypin, A.A., Kravtsov, A.V., Wechsler, R.H., Primack, J.R., & J.S. Bullock. 2002, ApJ, 581, 799

Weldrake, D.T.F., de Blok, W.J.G., & Walter, F. 2003, MNRAS, 340, 12